PCCP

Accepted Manuscript

ROYAL SOCIETY OF CHEMISTRY

rsc.li/pccp

View Article Online
DOI: 10.1039/C7CP02248D

Journal Name

ARTICLE

Structure-properties relationship of blue solid state emissive phenanthroimidazole derivatives

Received 00th January 20xx,
Accepted 00th January 20xx

DOI: 10.1039/x0xx00000x

www.rsc.org/

Agne Ivanauskaite,[a] Ramunas Lygaitis,[a] Steponas Raisys,[b] Karolis Kazlauskas,[b] Gediminas Kreiza,[b] Dmytro Volyniuk,[a] Dalius Gudeika,[a] Saulius Jursenas[b] and Juozas V. Grazulevicius[a,†]

Seven new derivatives of phenanthro[9,10-d]imidazole having differenet substituents at the 1st and the 2nd positions of phenanthroimidazole moiety were synthesized and characterized. The comparative study of their properties was performed employing thermal, optical, electrochemical and photoelectrical measurements. Properties of the newly synthesized compounds were compared withose of earlier reported derivatives of phenanthroimidazole and several interesting new findings were disclosed. Density functional theory calculations accompanied by optical spectroscopy measurements have shown the possibility to tune the emission properties (excited-stated decay rate, fluorescence quantum yield *etc*) of phenanthro[9,10-d]imidazole derivatives *via* attachment of different substituents to the 1st and the 2nd positions. The most polar and bulky substituents linked to the 2nd position were found to have the greatest impact on the emissive properties of compounds causing i) fluorescence quantum yield enhancement of dilute liquid and solid solutions (up to 97%), ii) suppression of intramolecular torsion-induced nonradiative excited-state relaxation in rigid polymer films as well as iii) inhibition of aggregation-promoted emission quenching in the neat films. Most of the studied compunds exhibited ambipolar charge transport character with comparable drift mobilities of holes and electrons. The highest hole and electron mobilities approaching 10^{-4} $cm^2/V{\cdot}s$ were observed for the derivative having triphenylamino group at the 1st position of imidazole ring and phenyl group and the 2nd position The estimated triplet energies of phenanthro[9,10-d]imidazole compounds were found to be in the range of 2.4-2.6 eV which is sufficiently high to ensure effective energy transfer to yellow/red emitters.

INTRODUCTION

Organic light-emitting devices (OLEDs) are of great interest because of their present and potential applications in next generation full-color flat-panel displays and solid-state light sources.[1,2] Deep blue emitting emitters with the balanced mobilities of holes and electrons and with high triplet energies may be employed as hosts for green (G), yellow (Y) and red (R) phosphorescent emitters.[3] Achieving of high performance R, Y, G and blue electroluminescence (EL) based on simple materials and simplification of the structures of OLEDs are the important issues. For the preparation of the multi-functional electroactive materials, which can be employed not only as blue emitters, but also as hosts for efficient G, Y and R OLEDs, we propose the following design strategy of molecular materials: (i) the compounds have to contain hole transporting (donor) and electron transporting (acceptor) moieties and to exhibit high photoluminescence quantum yields (Φ_F) in the solid state; (ii) acceptor and donor moieties should be able to form electron and hole transporting channels in the solid layers of the materials (iii) to obtain deep blue emission, the charge transfer property of donor-acceptor molecules has to be relatively week since strong donor-acceptor interaction can cause red shift of emission; (iv) the difference between singlet and triplet energies (ΔE_{ST}) has to be small to ensure that triplet excited state energy is high enough to excite a dopant.[3,4]

Color quality and stability of blue phosphorescent OLEDs are often not sufficient.[5] The preparation of blue multifunctional compounds exhibiting high luminescence quantum yields, balanced charge transport properties and high thermal and morphological stability remains one of the challenging topics.[6] Usually, electron-transporting properties of organic semiconductors are inferior relative to hole-transporting properties, especially for blue emitting compounds.[7] One of the basic requirements for blue emitters is their enhanced electron affinities which enable to achive balanced charge injection and transport.[8,9] Compounds having heteroaromatic moieties, such as pyridine,[10] quinolone[11] and oxidazole[12] were reported to show good electron injection and transport properties, however these materials showed low luminescence quantum yields. 1,3,5-Tris(*N*-phenylbenzimidazol-2-yl)benzene (TPBi),

[a] Department of Polymer Chemistry and Technology, Kaunas University of Technology, Radvilenu pl. 19, LT-50254 Kaunas, Lithuania Fax: +37037 300152; Tel: +37037 300193.
[b] Institute of Applied Research, Vilnius University, Sauletekio 3, LT-10257 Vilnius, Lithuania.
† E-mail address: juozas.grazulevicius@ktu.lt (Juozas Vidas Grazulevicius).
Electronic Supplementary Information (ESI) available: [Experimental section, NMR, IR, UV/FL spectra of compounds, TOF transients for hole and electron transport, TGA and DSC curves, spatial distribution of frontier orbitals, cyclic voltammograms.]. See DOI: 10.1039/x0xx00000x

containing three 1-phenylbenzimidazole moieties linked by benzene ring, is widely used in OLEDs as electron-injecting and hole-blocking compound.[13] However, TPBi can not be used as emitter. It emits in the ultraviolet region with the intensity maximum at 368 nm. In addition, it has too large barrier for injection of holes.

For the design of efficient fluorescent emitter a suitable extent of intramolecular charge transfer (ICT) has to be secured by linking a donor (D) and acceptor (A) moieties.[14] This approach often gives the additional advantage, i.e., bipolar charge transporting property, which is beneficial for the improvement of characteristics of OLEDs.[15] The problem that arises in the design of deep-blue emitters is that the direct linkage between D and A moieties unavoidably increases the conjugation length, which can lead to red shift and broadening of the emission band. Therefore, efficienct deep-blue OLEDs satisfying the National Television System Committee standard color coordinates are rather rare.[16] To limit the ICT induced emission into blue region, the strength of donors and acceptors along with short π-conjugation linkage in organic luminogens are important aspects.[17] The longer conjugated bridge between donor and acceptor units of emitters is also a reason for bathochromic shifts in emission wavelength. Thus, the major challenge in the design strategy D-A-D compounds is to limit emission in deep blue region with short communication length between donor and acceptor.[18,19,20] Due to high luminescence quantum yields, high thermal stability, and relatively high triplet energies, phenanthroimidazole (PI) derivatives were reported to be useful as emitters or host materials.[21] Using PI moiety it is possible to design and obtain sky-blue and deep blue fluorescent emitters with fine color purities.[4,22] PI can act as an electron-acceptor when linked to electron-donor moiety, thus forming bipolar materials.[23] Deprotonation of NH group of imidazole moiety allows attaching wide variety of substituents, which can be capable to inhibit strong π-π stacking and molecular interactions in the solid state.[24] Introduction of electron-deficient PI units is known to effectively enhance electron injection and transport ability while allowing to adjust ionization potentials of compounds.[25]

In this work, we employ the D-A strategy to develop efficient deep-blue emitters by exploiting the merits of phenanthro[9,10-d]imidazole chromophore. Acting as a π-acceptor PI can be combined with an electron donor to form bipolar compounds and at the same to retain only weak intramolecular charge transfer. Bipolar molecules are expected to feature ambipolar charge transfer, therefore, both electron and hole transport can be realized. In addition, we evaluate radiative and non-radiative relaxation processes of PI derivatives with different polar substituents at 1st and 2nd position in various media such as solution, polymer matrix with low concentration of investigated compounds and in the neat films. Also, the influence of radiative and non-radiative processes on fluorescence quantum yield and absorption intensity is assessed. Phosphorescence measurements allowed estimating energy level of triplet state. As the bulk and sterically hindered molecular configuration is expected to effectively enhance photoluminescence quantum yield,[26] the impact of different substituents to packing specificity in the neat films is estimated. We expect the rigid PI fragment to be beneficial for the thermal and morphological stability without sacrificing good electron-transport ability and high triplet energy.

RESULTS AND DISCUSSION

Synthesis and characterization

All ten derivatives of phenanthroimidazole were synthesized in one-pot procedure as shown in Scheme 1. The synthesized derivatives were identified by mass spectrometry, ^{1}H, ^{13}C nuclear magnetic resonance (NMR) (see Supporting Information), infrared (IR) spectroscopy and element analysis. The materials were soluble in common organic solvents such us chloroform, toluene, acetone *etc*. Transparent thin films of these materials could be prepared by spin coating from solutions or by vacuum evaporation.

Scheme 1. Synthesis of phenanthroimidazole derivatives **1-10**.

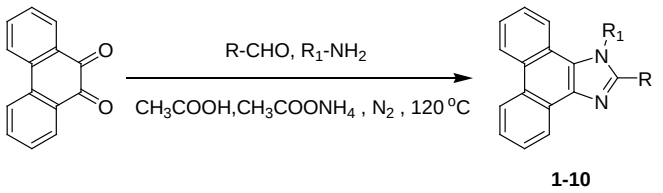

1-10

	1	2	3	4	5
R					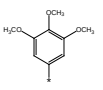
R_1	H	H			

	6	7	8	9	10
R					
R_1					

Thermal properties

Thermal properties of the synthesized compounds were studied by thermal gravimetric analysis (TGA) and differential scanning

View Article Online
DOI: 10.1039/C7CP02248D

calorimetry (DSC) under a nitrogen atmosphere. The data are presented in Table 1.

Table 1. Thermal characteristics of compounds **1-10**.

Compound	**1**	**2**	**3**	**4**	**5**	**6**	**7**	**8**	**9**	**10**[27]
T_m [°C] (1st heat)	325	297, 297[c)]	206, 206[c)]	200	207	200	227	273, 273[c)]	286	281
T_g [°C] (2nd heat)	-	135	65	-	82	82	-	-	-	-
T_{cr} [°C]	303[a)]	185[b)]	135[b)]	117[a)]	-	-	165[a)]	191[a)]	222[a)]	227[a)]
T_{ID} [°C]	330	342	344	350	380	381	337	315	430	420

[a)] T_{cr} is crystallization temperature determined during the cooling scan, [b)] T_{cr} is crystallization temperature determined during the 2nd heating scan; T_m is melting point; c) T_m is melting point recorded during the 2nd heating scan; T_g is glass transition temperature, T_{ID} is 5% weight loss temperature, recorded at scan rate 20 °C/min, N_2 atmosphere.

All the compounds (**1-10**) demonstrated high thermal stability. The initial 5% weight loss temperature (T_{ID}) ranged from 315 to 420 °C, as confirmed by TGA (Figure S1a, Supporting Information). T_{ID} of compounds **3-6** increased with the increasing number of methoxy groups in the molecules. This observation can apparently be explained by the enhancement of intermolecular interaction due to hydrogen bonding. T_{ID} of **7** containing trifluoromethyl substituents is lower by approximately 30 °C compared to that of compound **3** having no substituents at *para* positions of phenyl substituents. This difference may be attributed to the plasticizing effect of trifluoromethyl groups. Compounds **1** and **2** bearing hydrogen atom at the 1st position of phenanthroimidazole moiety have lower T_{ID} as compared to that of compound **3** possessing phenyl group at this position. This observation can be explained by the higher molecular weight of compound **3**, which predetermines stronger intermolecular interaction. Compounds **9** and **10** have the highest T_{ID} (430 and 420 °C, respectively) compared to compounds **1-8**. This observation again can be explained by the higher molecular weight of compounds **9** and **10**.

All the synthesized compounds (**1-10**) were obtained as crystalline materials as confirmed by DSC, however some of the materials could be converted to amorphous phase by cooling the melted samples. DSC thermograms of **5** shown in Figure 1 confirm this statement.

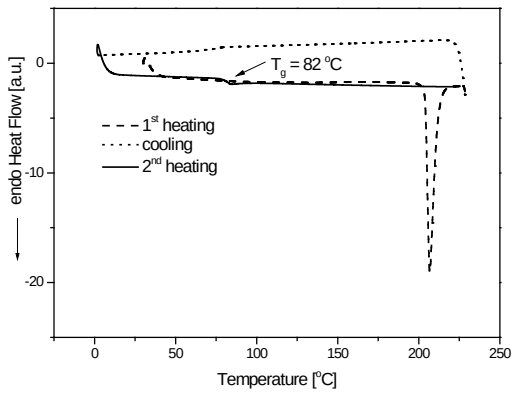

Figure 1. DSC curves of compound **5**.

When a crystalline sample of **5** was heated, melting point temperature (T_m) was recorded at 207 °C. When the molten sample was cooled down, it formed an amorphous material with glass transition temperature (T_g) of 82 °C. Compound **6** demonstrated the similar behavior during the DSC test. When its crystalline sample was heated, T_m was observed at 200 °C. When the melt sample was cooled down, it formed glass with T_g of 82 °C.

Compounds **1**, **4**, **7**, **8**, **9** and **10** demonstrated different behavior during the DSC experiments. Thermograms of compound **8** are shown in Figure S1b as an example. When the crystalline sample was heated, an endothermic peak due to melting was observed at 273 °C. When the melt sample was cooled down, its crystallization was observed at 191 °C to form the same crystals, which were obtained by crystallization from solution. The derivatives **1**, **4**, **7**, **9** and **10** demonstrated the similar behavior during the DSC tests (Table 1).

Compound **3** (Figure S1c, Supporting Information) demonstrated different behavior during the DSC experiments. When the crystalline sample was heated, endothermic peak due to T_m was observed at 206 °C. When the molten sample was cooled down, it formed glass with T_g of 65 °C followed by crystallization at 135 °C. Compound **2** demonstrated the similar behavior during the DSC test.

T_g of compound **2** having unsubstituted NH group is higher compared to those of compounds **3** and **5**, having phenyl groups at the 1st position of phenanthroimidazole moiety. This effect is apparently determined by the enhanced intermolecular interaction in the sample of **2** due to hydrogen bonds formed by NH groups. Compound **5** containing 3,4,5-trimethoxyphenyl group showed higher T_g by 17 °C compared to **3**, which at the 2nd position of phenanthroimidazole has phenyl group.

Density functional theory calculations

Geometry optimization of compounds **1-10** in the gas phase was performed using density functional theory (DFT) calculations at the B3LYP/6-31G* level as implemented in the Gaussian 09 software package.[28] Transition energies and oscillator strengths of the compounds were calculated using time-dependent DFT (TD-DFT) approach. The parameters involving the lowest singlet and triplet states are summarized in Table 2.

View Article Online
DOI: 10.1039/C7CP02248D

Table 2. Calculated transition energies, wavelengths and oscillator strengths for the 1st spin-allowed and spin-forbidden transition of compounds **1-10**.

	$S_0 \rightarrow S_1$			$S_0 \rightarrow T_1$	
Compound	E[a] (eV)	λ[b] (nm)	f[c]	E[a] (eV)	λ[b] (nm)
1	3.666	338.25	0.400	2.653	467.29
2	3.649	339.77	0.462	2.654	467.24
3	3.723	333.02	0.303	2.727	454.59
4	3.666	338.17	0.032	2.721	455.65
5	3.649	339.81	0.127	2.699	459.33
6	3.675	337.39	0.214	2.705	458.39
7	3.382	366.56	0.053	2.658	466.54
8	3.425	361.97	0.082	2.646	468.67
9	3.346	370.59	0.929	2.577	481.22
10	3.564	347.87	0.106	2.724	455.10

[a] Transition energy. [b] Transition wavelength. [c] Oscillator strength.

The compounds bearing substituents at the 2nd position only (**1** and **2**) exhibited planar molecular structure (Figure 2), which can result in remarkable fluorescence quenching at high compound concentrations, e.g. in the neat films. The additional substitution of the phenanthroimidazole moiety by phenyl group at the 1st position (**3**-**10)** induced large distortions to the molecular geometry causing 75° and 30° twist angles of the phenyl groups linked to the 1st and 2nd positions, respectively, in regard to phenanthroimidazole core (Figure S2, Supporting Information). The twisted molecular geometry is likely to prevent close packing of the molecules at increased concentrations, and thus can suppress fluorescence quenching in the neat films.

The calculated highest occupied molecular orbital (HOMO) was found to be spread over the entire molecule (except for the highly twisted phenyl moiety at the 1st position) for all the studied PI compounds, whereas the lowest unoccupied molecular orbital (LUMO) for majority of the compounds was more shifted towards the substituents (Figure 2 and Figure S2, Supporting Information). This was particularly well observed in the case of compounds having trifluoromethylphenyl substituents (**7**, **8**) due to their strong electron-accepting character. The quite opposite behavior, i.e. shift of the LUMO towards phenanthroimidazole core, was observed for triphenylamino-substituted derivative **9** as a result of the pronounced electron-donating property of this substituent. Generally, rather good overlap of electron wave functions in HOMO and LUMO revealed by DFT predicts fairly high oscillator strengths, which translate to high fluorescence quantum yields, as well as large singlet-triplet energy splittings of 0.7–1.0 eV (Table 2). Somewhat reduced f for compounds **4**, **7** and **8** can be justified by less overlapped HOMO and LUMO due to the emergence of the additional orbital transitions with charge transfer character.

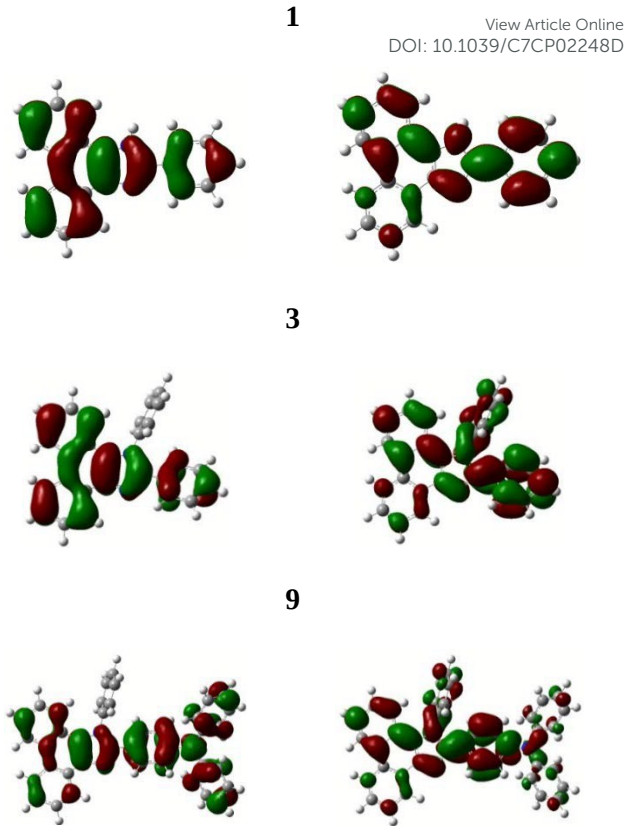

Figure 2. HOMO and LUMO for compounds **1**, **3** and **9** as calculated by DFT using B3LYP/6-31G* basis set. Frontier molecular orbitals of the rest compounds can be found in Figure S2 in Supporting Information.

Optical and photophysical characterization

The impact of various substituents introduced at the 1st and 2nd positions of PI has been assessed by evaluation of their optical properties. The properties of the PI derivatives observed for dilute solutions or for dispersions in rigid polymer matrices at low compound concentration allowed to reveal the influence of intramolecular mechanisms, whereas the results acquired for the neat films enabled to evaluate the contribution of intermolecular interactions, e.g., molecular packing and exciton migration induced excitation relaxation. Obvious differences in the polarity and steric properties of the substituents were shown to readily affect radiative and nonradiative relaxation processes of the PI compounds implying a possibility to tune their optical properties.

Figure S3 (Supporting Information) shows near-band-edge absorption spectra of dilute dimethylformamide (DMF) solutions of the PI derivatives. Compounds **1**-**8** exhibit similar absorption spectra with the 0th vibronic peak of the lowest energy band ranging from 360 to 366 nm (see Table 3). The slight variation can be attributed to a different polar and steric character of the substituents affecting extent of the electron delocalization. Generally, the absorption spectra of the PI compounds are red shifted by *ca.* 20 nm as compared to that of phenanthrene[29] due to the enhanced conjugation ensured by 2-phenylimidazole group. The absorbance of the lowest energy band of the phenyl- or methoxyphenyl-substituted PI

Journal Name ARTICLE

View Article Online
DOI: 10.1039/C7CP02248D

compounds **1**-**6** is found to be in the range of (7.4–11.5)×10^3 L·mol^{-1}·cm^{-1}. The increasing polarity of the substituents is observed to enhance the absorbance, *i.e.,* 1.5-fold enhancement is achieved for carbazole and $–CF_3$ substituents (compounds **10**, **7**, **8**), whereas 3-fold enhancement is attained in the case of diphenylamino group (compound **9**). The enhancement is accompanied by the significant broadening of the absorption spectrum, which is particularly noticeable in the compounds **9** and **10**. The increase of absorbance with increasing electron donating ability of the substituents is typical of D-A type molecules and is due to the increased transition dipole moment.

Table 3. Optical properties of 10^{-5} M DMF solutions, 0.5 wt% molecular dispersions in PS and of the neat films of PI derivatives. Phosphorescence properties were evaluated for the films of 2 wt% molecular dispersions in PMMA additionally doped with 25 wt% of benzophenone.

Compound		**1**	**2**	**3**	**4**	**5**	**6**	**7**	**8**	**9**	**10**
DMF solution											
Φ_F[a])	%	57	51	59	56	65	66	78	67	81	61
Abs[b])	$L·mol^{-1}cm^{-1}$	11540	9330	9900	7360	8500	8550	15880	15090	29800	13460
Abs_{max}[c])	nm	364	366	361	363	363	363	360	360	365	370
Fl_{max}[d])	nm	379 392	384 392	374 390	387 392 401	380 392	380 392	408	421	424	403
τ[e])	ns	6.8	6.7	6.9	6.7	5.8	6	2.1	2	1.8	4.3
τ_r[f])	ns	11.9	13.1	11.7	12	8.9	9.1	2.7	3	2.2	7
τ_{nr}[f])	ns	15.8	13.7	16.8	15.2	16.6	17.6	9.5	6.1	9.5	11
0.5 wt% PS film											
Φ_F[a])	%	63	55	64	55	84	71	90	84	97	80
Fl_{max}[d])	nm	376 394	379 396	370 389	377 394	376 393	376 394	395	403	408 423	384 403
τ[e])	ns	7.1	7	6.9	7.1	6.1	6.1	2.6	2.4	1.5	4
τ_r[f])	ns	11.3	12.7	10.7	12.9	7.2	8.6	2.8	2.8	1.5	5
τ_{nr}[f])	ns	19.3	15.5	19	15.8	37.9	21	25.6	14.7	49.3	20
Neat film											
Φ_F[a])	%	9	4	12	8	22	22	26	12	23	17
Abs_{max}[c])	nm	367	365	364	366	365	365	363	368	357	375
Fl_{max}[d])	nm	402 423	402	377 395 576	385 399 594	405	403	431	436	433	413
τ[g])	ns	0.45 [36%] 1.34 [56%] 5.45 [8%]	0.19 [56%] 1.11 [32%] 6.13 [12%]	0.06 [17%] 1.17 [42%] 3.47 [41%]	0.23 [21%] 0.91 [50%] 2.04 [29%]	0.36 [6%] 2.61 [65%] 7.51 [29%]	2.78	0.69 [20%] 2.70 [46%] 7.66 [34%]	1.40 [12%] 2.87 [79%] 6.39 [9%]	0.25 [58%] 1.28 [37%] 3.53 [5%]	0.25 [28%] 0.87 [66%] 3.29 [6%]
τ_a[h])	ns	1.3	1.2	1.9	1.1	3.9	2.8	4	3	0.8	0.8
2 wt% PMMA film with 25 wt% of BP											
$Phos_{max}$[i])	nm	-	481	495	493	507	506	516	520	490	510
E_T[j])	eV	-	2.58	2.51	2.52	2.45	2.45	2.40	2.38	2.53	2.43
ΔE_{ST}[k])	eV	-	0.69	0.85	0.77	0.85	0.85	0.74	0.69	0.51	0.80

[a]) Fluorescence quantum yield. [b]) Absorption intensity at lowest energy absorption band maximum. [c]) Lowest energy absorption band maximum. [d]) Fluorescence band maxima at vibronic peaks. [e]) Fluorescence lifetime at the highest vibronic peak of fluorescence band. [f]) τ_r – radiative decay time, τ_{nr} non-radiative decay time. [g]) Fluorescence lifetime measured at fluorescence band maximum. Fractional contribution (*f*) to the total fluorescence intensity is given in the parentheses. [h]) Average fluorescence lifetime calculated by $\tau_a = \Sigma\ \tau_i \times f_i$. [i]) Phosphorescence maximum at 0[th] vibronic replica. [j]) Energy level of the triplet state derived from $Phos_{max}$. [k]) Singlet-triplet energy splitting.

The solutions of phenyl- or methoxyphenyl-substituted PI compounds **1**-**6** in DMF exhibit fluorescence in blue and ultraviolet (UV) spectral region with emission maxima ranging from 374 nm to 401 nm and with fluorescence quantum yields of 51–66%. Fluorescence spectra express noticeable vibronic progression indicating rigid molecular backbone of PI. Conversely, the fluorescence spectra of the solutions of compounds **7**, **8** and **9** contain no vibronic replicas and are more Stokes shifted implying enhanced solvation effect induced by the presence of more polar substituents (Figure S3, Supporting Information). The compounds also exhibit somewhat higher fluorescence quantum yields of 78, 67 and 81%, respectively, what nicely correlates with increased absorbance (see Table 3).

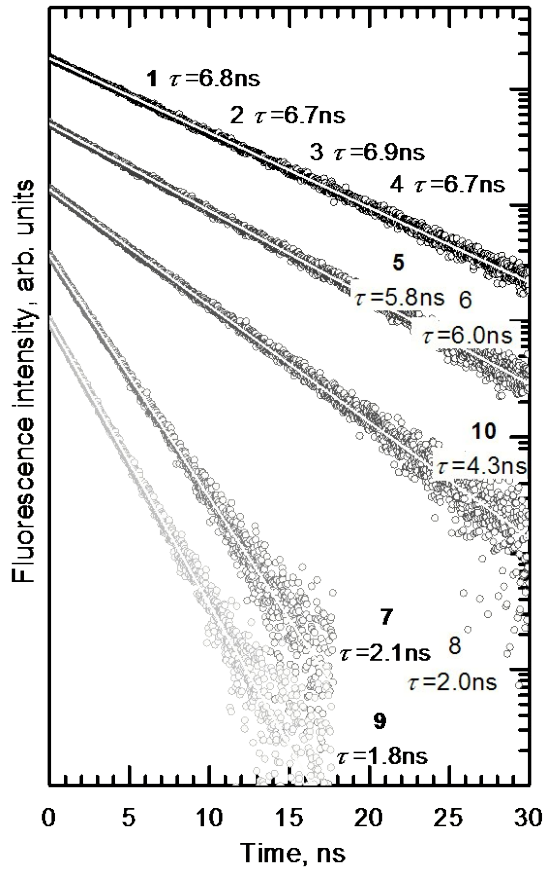

Figure 3. Fluorescence transients of the solutions of PI derivatives **1**, **5**, **7**, **9**, and **10** in 10^{-5} M DMF with fluorescence lifetimes of each compound indicated. The intensity of transients is scaled and arbitrarily shifted for clarity.

Fluorescence transient measurements for DMF solutions of the phenyl- and methoxyphenyl-substituted compounds **1**-**4** revealed mono-exponential decays with the fluorescence lifetime (τ) of ~6.8 ns (Figure 3). Trimethoxyphenyl-substituted compounds **5** and **6** expressed slightly shorter τ of ~5.9 ns, whereas the compounds with carbazole (**10**), trifluoromethylphenyl (**7**, **8**) and triphenylamino (**9**) substituents showed even more rapid decay with τ of 4.3, 2.1, 2.0 and 1.8 ns, respectively.

To estimate the relative contribution of radiative and nonradiative relaxation processes in the excited state deactivation and determine the governing mechanism, the radiative (τ_r) and nonradiative (τ_{nr}) decay time constants were calculated. The calculated constants ($\tau_r = \tau/\Phi_F$, $\tau_{nr} = \tau/(1-\Phi_F)$) revealed similar τ_r = ~12.2 ns and τ_{nr} = ~15.4 ns for the compounds **1**, **2**, **3** and **4**. The increased polarity of the substituents was found to strongly affect τ_r of the PI derivatives while influencing τ_{nr} at a much lesser degree. Particularly, for trimethoxyphenyl-substituted compounds (**5**, **6**) τ_r was shortened by 25% (to 9.0 ns), whereas τ_{nr} increased by only 10% (up to ~17.0 ns). Introduction of even more polar trifluoromethylphenyl and triphenylamino substituents (compounds **7**, **8** and **9**) resulted in the remarkable 3-fold enhancement of radiative decay rate, *i.e.* 3-fold reduction in τ_r, yet less than 2-fold decrease in τ_{nr}. Thereby, for compounds **7**, **8** and **9** τ_r was reduced down to ~2.6 ns, whereas τ_{nr} only down to ~8.4 ns.

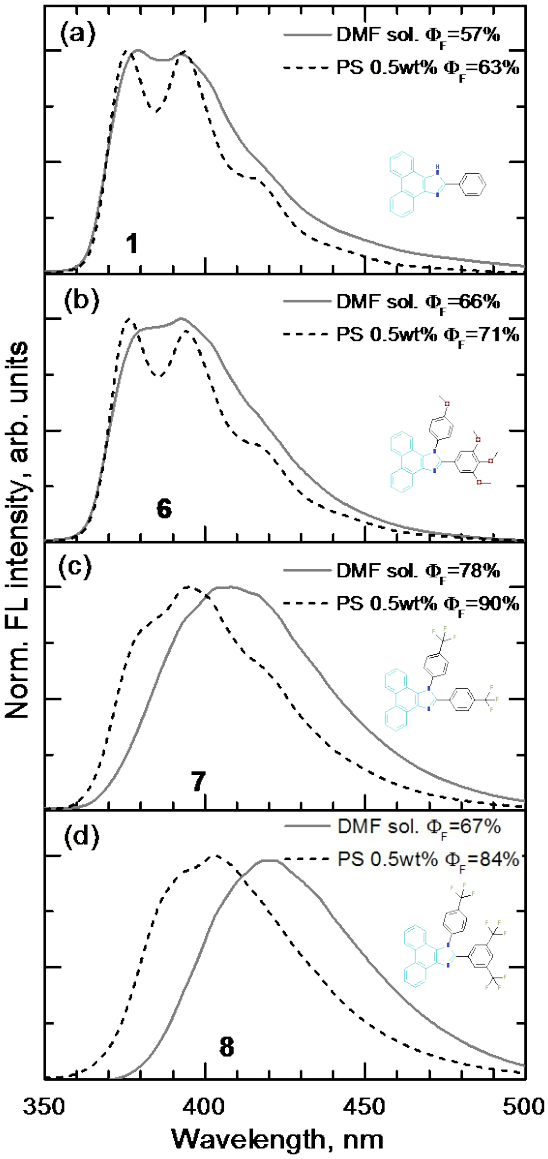

Figure 4. Normalized fluorescence spectra of 10^{-5} M DMF solutions and of 0.5 wt% molecular dispersions in PS of PI derivatives **1** (a), **6** (b), **7** (c) and **8** (d). Fluorescence quantum yields are indicated.

It is known that compounds bearing relatively small and flexible groups, such as phenyl groups linked to the 1st and 2nd position of phenanthroimidazole moiety, are prone to nonradiative deactivation due to the effective low-frequency vibronic mode (twist and torsion) coupling to the ground state.[30,31] While being efficient in the non-viscous media, e.g. solutions, the intramolecular torsions are highly suppressed in the environments of high viscosity, e.g. rigid polymer matrices.[32,33] Therefore, to elucidate the influence of intramolecular torsions of the various substituents on the optical properties of the compounds they were embedded into rigid polystyrene (PS) matrix at low concentration. Estimated fluorescence quantum

View Article Online
DOI: 10.1039/C7CP03948D

yield of all the compounds embedded into PS matrix showed 10-20% enhancement as compared to that observed for DMF solutions (Table 3). The increase of Φ_F is attributed to the restriction of intramolecular torsions and suppression of torsion-induced nonradiative excited state deactivation.[34] The small increase in Φ_F well correlates with the slightly longer fluorescence lifetimes estimated for the compounds dispersed in PS matrix. Importantly, although radiative τ_r of the dispersions in PS remains almost unchanged, τ_{nr} is enlarged significantly as compared to that for solutions. A particularly marked increase of τ_{nr} (by a factor of 2.5-5) is attained for the PI compounds bearing highly polar trifluoromethylphenyl and triphenylamino substituents (compounds **7**, **8** and **9**). The considerably suppressed nonradiative decay pathway can be unambiguously attributed to increased restriction of intramolecular torsions upon incorporation of the compounds into rigid PS matrices.

Fluorescence spectra of the films of dispersions of compounds **1**-**6**, **9** and **10** in PS were found to be similar to those observed for dilute solutions. Better resolved vibronic progressions for dispersions in PS were caused by the increased rigidity of the surrounding environment (Figure 4a and 4b). Conversely, the fluorescence spectra of compounds **7** and **8** dispersed in PS matrix were blue shifted up to 18 nm as compared to those observed for solutions (Figure 4c and 4d). The blue shift is most likely caused by the change in the polarity of the surrounding medium. Taking into account that PS is much less polar than DMF, stabilization of the excited state in PS is relatively weaker, and thus, the spectrum appears at shorter wavelengths.

Absorption spectra of the neat films of phenanthroimidazoles (Figure S4, Supporting Information) were found to be very similar to those of the dilute solutions with a spectral shift of the lowest energy band of only few nanometers. The absorption band of the films of compounds **7** and **8** bearing trifluoromethyl substituents exhibited slightly larger redshift (up to 8 nm, see Table 3) likely due to increased intermolecular interactions in the solid state facilitated by polar trifluoromethyl groups.

Although various substituents introduced at the 1st and 2nd positions of phenanthroimidazole moiety had a rather minor impact on the optical properties in dilute solutions, it strongly affected fluorescence properties of the solid samples (Figure S4, Supporting Information). Fluorescence spectra of the films of the compounds possessing phenyl and *tert*-butyl-phenyl groups (**1** and **2**) are located in the violet-deep blue region with the emission peak at 402 nm. The redshifted fluorescence spectra along with the dramatically reduced fluorescence quantum yield of the neat films of the compound (down to 4%) as compared to those of the dilute solutions imply strong aggregation induced quenching resulting from planar molecular backbone.[35] The introduction of the second phenyl group at the 1st position of phenanthroimidazole moiety (compound **3**) causes formation of excimer states, which are evident from the broad, structureless, long living (τ = 176 ns) fluorescence band at ~576 nm (Figure S4, Supporting Information). Although the attachment of additional phenyl ring enhanced Φ_F up to 12%, the emergence of the broad excimer band at long wavelengths is generally detrimental for the realization of blue emitters. The substitution of the 2-phenyl moiety with methoxy-phenyl (compound **4**) did not prevent formation of excimers either, conversely, caused excimer band boost in intensity in respect to molecular band. The excimer band of **4** was observed to shift to 594 nm also delivering shortened fluorescence lifetime of ~60 ns. The incorporation of three methoxy groups into the *meta*- and *para*-positions of the 2-phenyl moiety (**5**) effectively inhibited formation of eximers, and nearly tripled Φ_F (up to 22%). This result indicates that at least three methoxy groups are required to ensure effective intermolecular separation. The incorporation of the fourth methoxy group at the *para*-position of the 1-phenyl moiety (**6**) caused no visible changes in the optical properties (Table 3). Emission intensities for the neat films of both compounds **5** and **6** were found to peak at ~404 nm with Φ_F = 22%. Generally, the substitution of phenanthroimidazoles at the 1st position resulted in a twisted molecular structure, which suppressed aggregation induced fluorescence quenching, and thus enhanced Φ_F of the neat films (Table 3) as predicted by DFT calculations.

Compounds **7** and **8** possessing polar trifluoromethyl groups exhibited strongly Stokes-shifted fluorescence spectra with emission bands peaking at 431 and 436 nm, respectively (Figure S4, Supporting Information). As a result of the donor-acceptor type intramolecular interaction involving formation of charge transfer states, the vibronic modes were absent in the fluorescence spectra of both compounds (Figure S4, Supporting Information). Compound **7** with two identical trifluoromethyl substituents linked at the *para*- position exhibited Φ_F of 26% in the solid state, whereas compound **8** with two trifluoromethyl groups linked at the *meta*- position showed 2-fold reduced Φ_F. It is likely that the difference in Φ_F in the solid state is provoked by diverse molecular packing due to the different trifluoromethyl linking topology.

It was found that Φ_F of the carbazole-substituted phenantroimidazole derivative (**10**) is enhanced as compared to that of derivatives **1**, **2**, **3** or **4**, however out-of-plane twisted carbazole moiety is incapable of avoiding close molecular packing and excimer formation in the neat films. Weak excimer band as a long-wavelength slope was observed in the fluorescence spectrum of neat film of **10**. The average lifetime of this band was measured to be ~60 ns. It is worth noting that introduction of triphenylamino substituent had minor influence on the fluorescence spectrum of the film as compared to that of solution and allowed to effectively suppress excimer emission in the solid films with relatively high Φ_F (23%).

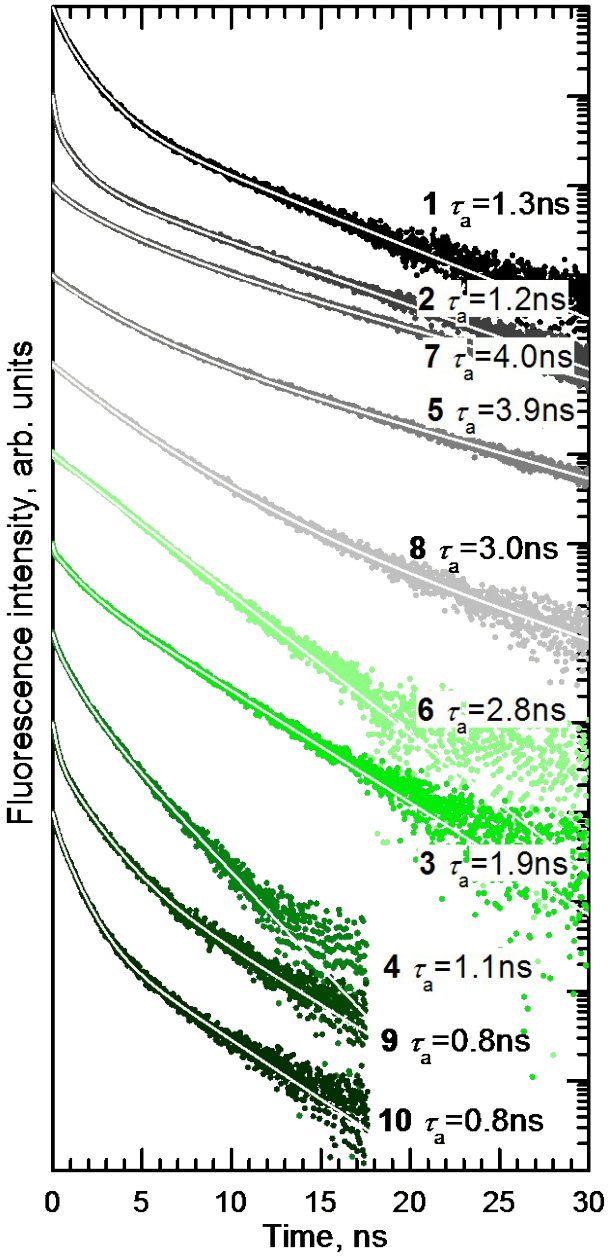

Figure 5. Fluorescence transients of the neat films of PI derivatives with average fluorescence lifetimes indicated. The intensity of each transient was arbitrarily shifted for clarity.

Fluorescence transients of the neat films of PI derivatives are shown in Figure 5. Generally, the transients exhibit non-exponential decay indicating dispersive exciton hopping through the localized states in the disordered media.[36,37] The fluorescence lifetimes were extracted by fitting the transients using multi-exponential decay model (Table 3). The average fluorescence lifetimes are indicated in Figure 5. For the neat films of most of compounds the average τ was significantly shorter as that found for solutions. The shortened lifetime is attributed to exciton migration (or energy transfer) in the condensed phase and migration-induced enhanced exciton quenching at non-radiative decay sites.[38,39] Interestingly, the films of compounds **7** and **8** with trifluoromethyl groups expressed prolonged τ as compared to those found for solutions. Taking into account considerably reduced Φ_F of the neat films, the prolonged τ can be caused by the enhanced radiative decay channel as a result of polar groups induced specific molecular packing.

Knowledge of the triplet energies of phenantroimidazole compounds is essential for their possible application, e.g. as host materials in light emitting devices. The triplet energies of the compounds were estimated from their phosphorescence spectra exhibiting relatively high intensity at room temperature due to the triplet sensitization method employed.[40] Triplet sensitizer, benzophenone (BP), featuring 100% intersystem crossing rate and high triplet energy (2.96 eV) was added to poly(methyl methacrylate) (PMMA) films with the dispersed phenantroimidazole compounds to foster singlet excitons conversion to triplets as well as their transfer to the triplet states of phenanthroimidazoles. PMMA films with 2 wt% of the investigated compounds and 25 wt% of BP were used in the phosphorescence measurements. The excitation wavelength was tuned to the absorption of BP (330 nm). Additionally, to avoid the interfering fluorescence signal in the background, phosphorescence spectra were recorded with the delay of 1 μs after the excitation pulse by using time-gated technique.

Phosphorescence spectra of the PI derivatives **6**-**10** are presented in Figure 6. The spectra of the compounds **2**-**5** were found to be almost identical to that of **6** and therefore are not show. Unfortunately, low phosphorescence quantum yield of compound **1** rendered its phosphorescence spectrum measurements impossible. All the compounds displayed phosphorescence in the green spectral region with the band maximum ranging from 490 to 550 nm. Phosphorescence spectra have similar shape as compared to fluorescence of DMF solution. The triplet energies of the compounds estimated from the band maxima of phosphorescence spectra are listed in Table 3. Based on this data singlet-triplet energy splitting of the phenanthroimidazoles was calculated from the fluorescence and phosphorescence spectra. ΔE_{ST} was found to vary from 0.51 to 0.85 eV for the studied compounds (Table 3). Such large ΔE_{ST} generally indicates a good overlap of the HOMO and LUMO molecular orbitals as it was predicted by DFT calculations. This observation also shows rather moderate influence of various substituents on the distribution of molecular orbitals in phenanthroimidazoles. Somewhat reduced ΔE_{ST} of 0.51 eV (due to the blue shifted phosphorescence spectrum) obtained for compound **9** bearing electron-donating triphenylamino unit is likely caused by the slightly reduced spatial overlap between HOMO and LUMO in the donor-acceptor type molecule (Figure 2).

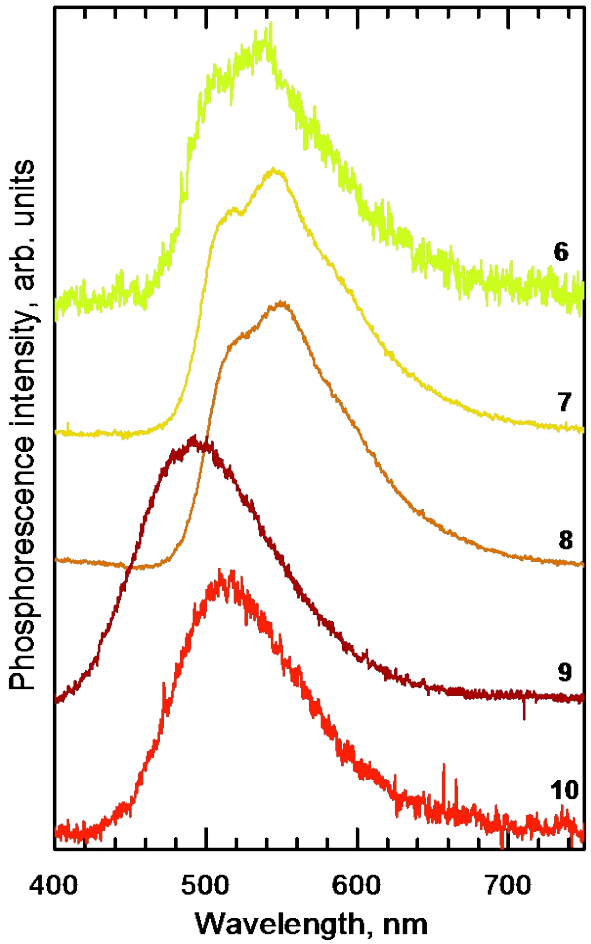

Figure 6. Phosphorescence spectra of the PI derivatives (**6-10**) at room temperature. The intensity of each spectrum was arbitrarily shifted for clarity.

Electrochemical properties

Electrochemical properties of the synthesized PI derivatives were investigated by cyclic voltammetry (CV). The results are presented in Table 4. The shape of cyclic voltammograms was found to be similar for all the studied compounds. During CV experiments **1-10** showed only quasi-reversible oxidation couple and no reduction waves (Figure 7, Figure S5, Supporting Information).

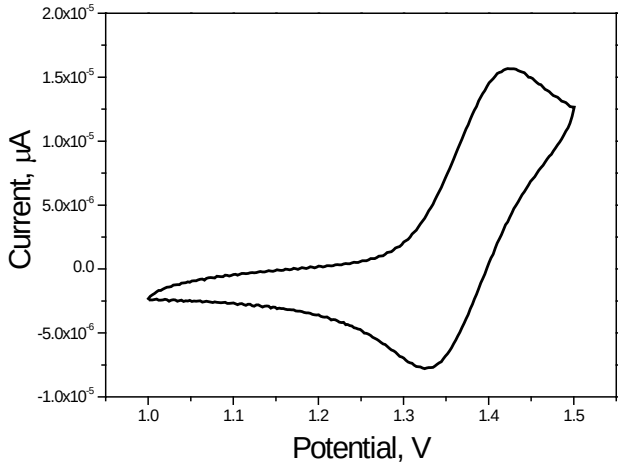

Figure 7. Cyclic voltammogram of dilute solution of compound **8** in dichloromethane at room temperature at sweep rate of 100 mV/s.

The oxidation potentials for the reversible oxidation are taken as the average of the cathodic and anodic peak potentials. The oxidation potentials for **1-10** were found to be 0.60-1.20 V.
The ionization potential values (IP_{CV}) were determined from the values of the first oxidation potential (E_p) with respect to ferrocene ($IP_{CV} = E_p + 4.8$ eV). IP_{CV} values of the compounds ranged from 5.20 to 5.80 eV. Compounds **9** and **10** having electron donating triphenylamino and carbazolyl groups at the 2nd position of PI moiety showed the lowest values of IP_{CV}. The highest IP_{CV} values were observed for compounds **7** and **8** containing trifluoromethyl substituents. The electron affinities (EA_{cv}) determined from the optical energy band gaps (E_g^{opt}) and ionization energy values ($EA_{CV} = -(|IP_{CV}| - E_g^{opt})$) were in the range of 2.19-3.37 eV. The calculated EA_{CV} ranged from 2.06 to 3.25 eV.

Table 4. Electrochemical and photoelectrical data of PI derivatives **1-10**.

Compound	1	2	3	4	5	6	7	8	9	10[27]
E_{ox} [V][a]	0.69	0.98	0.97	0.85	0.85	0.81	1.14	1.20	0.60	0.69
E_p [V][b]	0.49	0.78	0.77	0.65	0.65	0.61	0.94	1.00	0.40	0.49
E_g^{opt} [eV][c]	2.19	2.19	3.34	3.25	3.31	3.31	3.28	3.24	3.03	3.23
IP_{CV} [eV][d]	5.29	5.58	5.57	5.45	5.45	5.41	5.74	5.80	5.20	5.29
IP_{EP} [eV][e]	5.40	5.43	5.60	5.54	5.42	5.43	-	-	5.21	5.21
EA_{CV} [eV][e]	3.25	3.24	2.23	2.20	2.14	2.10	2.46	2.56	2.17	2.06

[a] onset oxidation potential *vs.* Ag/Ag^+, [b] E_p is onset oxidation potential *vs.* Fc/Fc^+ ($E_p = E_{ox} - E_{1/2}^{Fc/Fc+}$ ($E_{1/2}^{Fc/Fc+} = 0.20$ V *vs.* Ag/Ag^+)); [c] optical band gap, estimated from the edges of electronic absorption spectra ($E_g^{opt} = 1240/\lambda_{edge}$); [d] $IP_{CV} = -(E_p+4.8)$; [e] IP_{EP} is ionization potential of thin solid layers; [f] $EA_{CV} = -(|IP_{CV}| - E_g^{opt})$.

Photoelectrical properties

Photoelectron emission measurements of the layers of the studied compounds were performed in order to get solid state ionization potentials (IP_{EP}). Photoelectron emission spectra for solid layers of the compounds are plotted in Figure 8. The IP_{EP} values of the compounds were obtained at the points of crossing straight lines with x-axis. Solid-state IP_{EP} values ranged between 5.21-5.60 eV for compounds **1-6, 9, 10**. These values are not far from the work function of indium tin oxide anode. Therefore, good hole injection to functional layers in organic devices based on studied materials can be predicted. The IP_{EP}

View Article Online
DOI: 10.1039/C7CP02248D

values showed the similar tendencies as IP_{CV} values. The lowest IP_{EP} values were observed for compounds **9** and **10** having electron donating triphenylamino and carbazolyl groups at the 2nd position of PI moiety. The IP_{EP} values for trifluoromethyl substituted compounds **7** and **8** were not estimated, possibly, due to the limitation of photoelectron emission spectrometry performed in air (which is because of the absorbance of high energy UV radiation (with photon energy ≥6.0 eV) by oxygen in air). The IP_{EP} values for compounds **7** and **8** could be even higher than those estimated by CV measurements due to the increased intermolecular interactions in solid-state (Table 4). As a result, the photoelectron emission spectra were not recorded hence the IP_{EP} values were not estimated for these compounds.

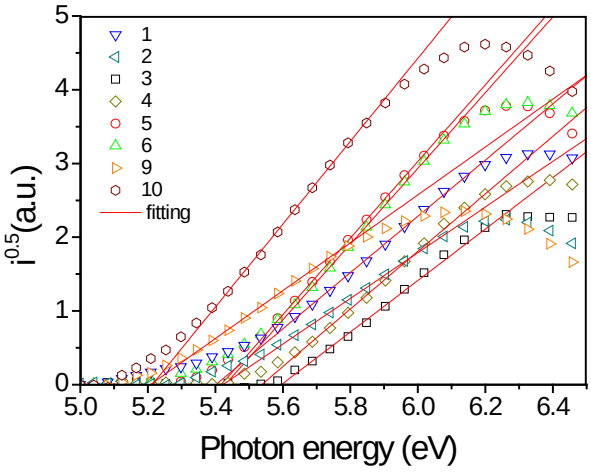

Figure 8. Photoelectron emission spectra of the solid state layers of compounds **1-6, 9, 10**.

To investigate influences of different substitutions of compounds on their charge-transporting properties, the time of flight (TOF) method was employed. Hole transport for the compounds **3-10** substituted at the both 1st and 2nd positions of PI were observed. Hole-transporting ability for compounds **1** and **2** substituted by phenyl group only at 2st position of PI was not proved by TOF apparently due to the weak donating ability of one phenyl moiety. Despite all studied compounds are based on the accepting phenanthroimidazole unit, electron transport was only observed for compounds **4-6, 9,10** substituted at both 1st and 2nd positions of PI by phenyl, methoxyphenyl, carbazolyl, or triphenylamino moieties. Attachement of electron-accepting trifluoromethyl groups to phenyl moieties of **7** and **8** did not induce electron-transporting ability to these compounds. In contrast to methoxy substitution in compounds **4-6**, trifluoromethyl substitution in compounds **7** and **8** apparently lead to the increase of electron hopping distance which restricted electron transport in the layers of these compounds.[41] Consequently, bipolar charge transport properties were observed for compounds **4-6, 9,10** substituted at the 1st position of PI by methoxyphenyl, carbazolyl, or triphenylamino moieties. Apparently, the different spatial frontier orbital distributions resulting from the different substitution of PI can be the reason for this observation.[42] Appropriate orbital overlap between the HOMOs and LUMOs of the molecules assist to hole and electron hopping between adjacent molecules resulting to the bipolar charge transport properties in the compounds **4-6, 9** and **10**. For example, the HOMOs and LUMOs of **9** are localized on both donating and accepting moieties (Figure 2). This indicates that the adjacent molecules should facilely achieve mutual contact with each other to obtain bipolar charge transport. In addition, C–H···π, O, N hydrogen bonds induced by methoxy groups of compounds **4-6** can have impact on the intermolecular interaction energies resulting in different values of the charge mobility.[43] Hole mobility values at electric fields of 0.5×10^5 – 5.5×10^5 V/cm for the compounds range between *ca.* 10^{-7}-10^{-4} cm^2/Vs depending on the substitutions (Figure 9). The highest hole mobility value of 2.74×10^{-4} cm^2/Vs at 4.23×10^5 V/cm was obtained for compound **9** being substituted by a strongly donating triphenylamino moiety. The hole transit times for the compounds **3-10** were well seen on log-log plots of TOF transients which displayed even low dispersity of hole transport for compounds **5, 9** and **10** (Figure S6, Supporting Information). Electron transport for compounds **4-6, 9, 10** was detected by TOF as the kink on photocurrent transients in the log–log for these compounds was seen (marked by red lines, Figure S6, Supporting Information). Electron mobility values for compounds **4-6**, **9** and **10** were found to be in the range from 3.7×10^{-7} to 8.8×10^{-5} cm^2/Vs at electric fields of 0.5×10^5 - 5.5×10^5 V/cm (Figure 9). Electron mobilities for PI-based compounds **4-6**, and **10** were obtained to be slightly higher than their hole mobilities at the same electric fields. Only for compound **9** hole mobility was found to be approximately by one order higher than its electron mobility apparently due to the presence of the strong donor i.e. triphenylamino unit (Figure 9). Electron transport for compounds **1-3, 7, 8** was not detected by the TOF measurements as the transit times on the related photocurrent transients were not seen for these compounds (Figure S6, Supporting Information). Despite rather low hole and electron mobilities of compounds **3-10** compared to those of organic semiconductors published before,[44] these values are comparable with charge mobilities of recently published effective OLED emitters.[45]

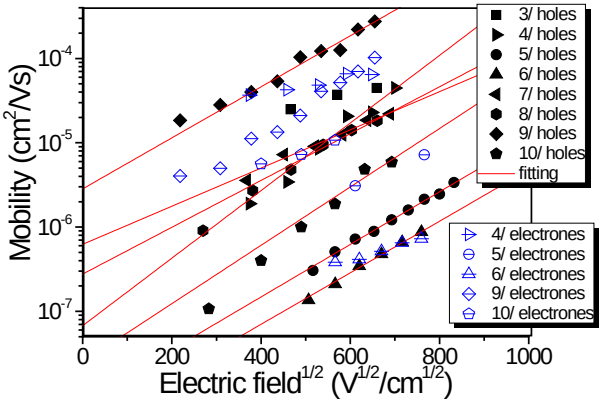

Figure 9. Visualization of the experimental charge mobilities of compounds **3-10**.

CONCLUSIONS

In conclusion, we have synthesized and investigated structure-property relationship of phenanthroimidazole derivatives by studying their thermal, photophysical, electrochemical and photoelectrical properties. Dilute liquid and solid solutions of phenanthroimidazole derivatives were found to emit in a deep blue spectral region (390-430 nm) with high fluorescence quantum yield (up to 97%). Increase of the polarity of the substituents linked to the 2nd position of phenanthroimidazole moiety enhanced absorption and fluorescence quantum yields of dilute solutions as a result of increased radiative decay rate. Incorporation of phenanthroimidazole compounds into rigid PS matrix revealed remarkable lengthening of nonradiative decay time accompanied by enhancement of fluorescence quantum yield due to the restriction of intramolecular torsions and suppression of torsion-induced nonradiative excited-state deactivation. This was particularly well pronounced for phenanthroimidazoles substituted with polar groups. A significant drop of fluorescence quantum yield of the neat phenanthroimidazole films (down to 4%) was obviously facilitated by planar phenanthroimidazole core promoting aggregation-induced emission quenching. However, the attachment of phenyl moiety at the 1st position as well as other bulky groups like methoxyphenyl or triphenylamino at the 2nd position of phenanthroimidazole moiety conditioned up to 6-fold boost in fluorescence quantum yield due to the sterical hindrance effects effectively suppressing aggregation. The D-A structure of the phenanthroimidazole compounds implied ambipolar charged carrier transport in their films with charge drift mobilities reaching 10^{-4} $cm^2/V{\cdot}s$. The triplet energies of phenanthroimidazoles revealed from phosphorescence measurements were found to be 2.4-2.6 eV below singlet manifold (in the green spectral region) ensuring effective energy transfer to yellow and red dopants.

Acknowledgements

This work was supported by the Research Council of Lithuania. (grant No TAP LLT-2/2017). D. Gudeika thanks for the support from the Lithuanian Academy of Sciences.

Notes and references

1 R. Y. Sun, N. C. Giebink, H. Kanno, B. W. Ma, M. E. Thompson and S. R. Forrest, *Nature,* 2006, **440**, 908.
2 R. P.Xu, Y. Q. Li and J. X, *J. Mater. Chem. C*, 2016, **4**, 9116.
3 C. Li, S. Wang, W. Chen, J. Wei, G. Yang, K. Ye, Y. Liu and Y. Wang, *Chem. Commun.,* 2015, **51**, 10632.
4 T. Shan, Y. Liu, X. Tang, Q. Bai, Y. Gao, Z. Gao, J. Li, J. Deng, B. Yang, P. Lu and Y.Ma, *ACS Appl. Mater. Interfaces,* 2016, **8**, 28771.
5 J. Jayabharathi, R. Sathishkumar, V. Thanikachalam and K. Jayamoorthy, *J. Lumin.,* 2014, **153**, 343.
6 S. Zhuang, R. Shangguan, H. Huang, G. Tu, L. Wang and X. Zhu, *Dyes Pigm.,* 2014, **101**, 93.
7 Z. Wang, P. Lu, S. Chen, Z. Gao, F. Shen, W. Zhang, Y. Xu, H. S. Kwok and Y. Ma, *J. Mater. Chem*., 2011, **21**, 5451.
8 M. S. Gong, H. S. Lee and Y. M. Jeon, *J. Mater. Chem.*, 2010, **20**, 10735.
9 S. Tang, M. R. Liu, P. Lu, H. Xia, M. Li, Z. Q. Xie, F. Z. Shen, C. Gu, H. Wang, B. Yang and Y. G. Ma, *Adv. Funct. Mater.,* 2007, **17**, 2869.
10 N. Li, P. Wang, S. L. Lai, W. Liu, C. S. Lee, S. T. Lee and Z. Liu, *Adv. Mater.,* 2010, **27**, 527.
11 S. Tao, L. Li, J. Yu, Y. Jiang, Y. Zhou, C. S. Lee, S. T. Lee, X. Zhang and O. Kwon, *Chem. Mater.,* 2009, **21**, 1284.
12 J. Huang, Q. Liu, J. H. Zou, X. H. Zhu, A. Y. Li, J. W. Li, Wu, S. Peng, J. B. Cao, Y. Xia, R. Bradley and D. D. C. Roncali, *J. Adv. Funct. Mater*., 2009, **19**, 2978.
13 S. C. Lo, N. A. H. Male, J. P. J. Markham, S. W. Magennis, P. L. Burn, O. V. Salata and I. D. W. Samuel, *Adv. Mater.,* 2002, **14**, 975.
14 (a) S. Chen, Y. Wu, Y. Zhao and D. Fang, *RSC Adv.* 2015, **5**, 72009; (b) X. Tang, Q. Bai, Q. Peng, Y. Gao, J. Li, Y. Liu, L. Yao, P. Lu, B. Yang and Y. Ma, *Chem. Mater.*, 2015, **27**, 7050.
15 B. Liu, J. Zhao, C. Luo, F. Lu, S. Tao and Q. Tong, *J. Mater. Chem. C,* 2016, **4**, 2003.
16 X. Yang, X. Xua and G. Zhou, *J. Mater. Chem. C,* 2015, **3**, 913.
17 J. Y. Hu, Y. J. Pu, F. Satoh, S. Kawata, H. Katagiri, H; Sasabe and J. Kido, *Adv. Funct. Mater.,* 2014, **24**, 2064.
18 Q. Zhang, J. Li, K. Shizu, S. Huang, S. Hirata, H. Miyazaki and C. Adachi, *J. Am. Chem. Soc.,* 2012, **134**, 14706.
19 (a) K. Shizu, H. Noda, H. Tanaka, M. Taneda, M. Uejima, T. Sato, K. Tanaka, H. Kaji and C.Adachi, *J. Phys. Chem. C,* 2015, **119**, 1291; (b) B. Wang, G. Mu, J.Tan, Z.Lei, J.Jin and L Wang, *J. Mater. Chem. C*, 2015, **3**, 7709.
20 (a) W. C. Chen, C. S. Lee and Q. X. Tong, *J. Mater. Chem. C,* 2015, **3**, 10957; (b) C. Li, J. Wei, J. Han, Z. Li, X. Song, Z. Zhang, J. Zhang and Y. Wang, *J. Mater. Chem. C*, 2016, **4**, 10120.
21 (a) F. Lu, Q. X. Tong, Q. D. Yang, J. Ye, M. Y. Chan and C. S. Lee, *Adv. Optical Mater.,* 2015, **3**, 1215; (b) T. Jadhav, J. M. Choi, B. Dhokale, S. M. Mobin, J. Y. Lee and R. Misra, *J. Phys. Chem. C,* 2016,**120**, 18487; (c) Z. Wang, P. Lu, S. Chen, Z. Gao, F. Shen, W. Zhang, Y. Xu, H. S. Kwok and Y. Ma, *J. Mater. Chem.,* 2011, **21**, 5451; (d) B. Wang, X. Lv, J. Tan, Q. Zhang, Z. Huang, W. Yi and L. Wang, J. Mater. Chem. C**,** 2016, **4**, 8473.
22 (a) W. C. Chen, Y. Yuan, G. F. Wu, H. X. Wei, L. Tang, Q. X. Tong, F. L. Wong, C. S. Lee, *Adv. Opt. Mater.,* 2014, **2**, 626; (b) Z. Wang, X. Li, K. Xue, H. Li, X. Zhang, Y. Liu, Z. Yu, P. Lu and P. Chen, *J. Mater. Chem. C,* 2016, **4**, 1886.
23 S. Zhang, L. Yao, Q. Peng, W. Li, Y. Pan, R. Xiao, Y. Gao, C. Gu, Z. Wang, P. Lu, F. Li, S. Su, B. Yang and Y. Ma, *Adv. Funct. Mater.,* 2015, **25**, 1755.
24 X. Yang, R. A. Jones, M. M. Oye, M. Wiester and R. J. Lai, *New J. Chem.,* 2011, **35**, 310.
25 Z. Wang, Y. Feng, H. Li, Z. Gao, X. Zhang, P. Lu, P. Chen, Y. Ma and S.Liu, *Phys. Chem. Chem. Phys.,* 2014, **16**, 10837.
26 Y. Yuan, J. X. Chen, W. C. Chen, S. F. Ni, H. X. Wei, J. Ye, F. L. Wong, Z. W. Zhou, Q. X. Tong and C. S. Lee, *Org. Electron.,* 2015, **18**, 61.
27 D. Gudeika, A. Ivanauskaite, R. Lygaitis, V. Kosach, D. Volyniuk, R. Butkute, A. P. Naumenko, V. Yashchuk and J. V. Grazulevicius, *J. Photochem. Photobio. A,* 2016, **315**, 121.
28 M. J. Frisch, G. W. Trucks, H. B. Schlegel, G. E. Scuseria, M. A. Robb, J. R. Cheeseman, G. Scalmani, V. Barone, B. Mennucci, G. A. Petersson, H. Nakatsuji, M. Caricato, X. Li, H. P. Hratchian, A. F. Izmaylov, J. Bloino, G. Zheng, J. L. Sonnenberg, M.;Hada, M. Ehara, K. Toyota, R. Fukuda, J. Hasegawa, M. Ishida, T. Nakajima, Y. Honda, O. Kitao, H. Nakai, T. Vreven, J., J. A. Montgomery, J. E. Peralta, F. Ogliaro, M. Bearpark, J. J. Heyd, E. Brothers, K. N. Kudin, V. N. Staroverov, T. Keith, R. Kobayashi, J. Normand, K. Raghavachari, A. Rendell, J. C. Burant, S. S. Iyengar, J. Tomasi, M. Cossi, N. Rega, J. M. Millam, M. Klene, J. E.Knox, J. B. Cross, V. Bakken, C. Adamo, J. Jaramillo, R. Gomperts, R. E. Stratmann, O. Yazyev, A. J.

View Article Online
DOI: 10.1039/C7CP02248D

Austin, R. Cammi, C. Pomelli, J. W. Ochterski, R. L. Martin, K. Morokuma, V. G. Zakrzewski, G. A. Voth, P. Salvador, J. J. Dannenberg, S. Dapprich, A. D. Daniels, O. Farkas, J. B. Foresman, J. V. Ortiz, J. Cioslowski and D. J. Fox, 2009, Gaussian 09, Revision B.01, Gaussian Inc., Wallingford CT, 2010.

29 R. González-Luque, L. Serrano-Andrés, M. Merchán and M. P. Fülscher, *Theor. Chem. Acc.,* 2003, **110**, 224.

30 Q. Peng, Y. Yi, Z. Shuai and J. Shao, *J. Am. Chem. Soc.,* 2007, **129**, 9333.

31 N. B. Shustova, T. C. Ong, A. F. Cozzolino, V. K. Michaelis, R. G. Griffin and M. Dincă, *J. Am. Chem. Soc.,* 2012, **134**, 15061.

32 E. Arbačiauskienė, K. Kazlauskas, A. Miasojedovas, S. Juršėnas, V. Jankauskas, W. Holzer, V. Getautis and A. Šačkus, *Synth. Met.,* 2010, **160**, 490.

33 S. Krotkus, K. Kazlauskas, A. Miasojedovas, A. Gruodis, A. Tomkeviciene, J. V. Grazulevicius and S. Jursenas, *J. Phys. Chem. C,* 2012, **116**, 7561.

34 K. Kazlauskas, G. Kreiza, E. Arbačiauskienė, A. Bieliauskas, V. Getautis, A. Šačkus and S.,Juršėnas, *J. Phys. Chem. C,* 2014, **118**, 25261.

35 V. Sivamurugan, K. Kazlauskas, S. Jursenas, A. Gruodis, J. Simokaitiene, J. V. Grazulevicius and S. Valiyaveettil, *J. Phys. Chem. B,* 2010, **114**, 1782.

36 R. Kersting, B. Mollay, M. Rusch, J. Wenisch, G. Leising and H. F. Kauffmann, *J. Chem. Phys.,* 1997, **106**, 2850.

37 R. R. Reghu, J. V. Grazulevicius, J. Simokaitiene, T. Matulaitis, A. Miasojedovas, K. Kazlauskas, S. Jursenas, P. Data, M. Lapkowski and P.Zassowski, *Dyes Pigm.,* 2013, **97**, 412.

38 R. Karpicz, S. Puzinas, S. Krotkus, K. Kazlauskas, S. Jursenas, J. V. Grazulevicius, S. Grigalevicius and V. Gulbinas *J. Chem. Phys.,* 2011, **134**, 204508.

39 T. Malinauskas, M. Daskeviciene, G. Bubniene, I. Petrikyte, S. Raisys, K. Kazlauskas, V. Gaidelis, V. Jankauskas, R. Maldzius, S. Jursenas and V .Getautis, *Chem. Eur. J.,* 2013, **19**, 15044.

40 S. Reineke and M. A. Baldo, *Scientific Reports,* 2014, **4**, 1.

41 I. I. Fishchuk, A. K. Kadashchuk, A. Vakhnin, Y. Korosko, H. Bassler, B. Souharce and U. Scherf, *Phys. Rev. B,* 2006, **73**, 115210.

42 D. Zhang, M. Cai, Z. Bin, Y. Zhang, D. Zhang and L. Duan, *Chem. Sci.,* 2016, **7**, 3355.

43 D. Gudeika, A. Bundulis, I. Mihailovs, D. Volyniuk, M. Rutkis and J. V. Grazulevicius, *Dyes Pigm.,* 2017, **140**, 431.

44 D. Gudeika, G. Sini, V. Jankauskas, G. Sych, J. V. Grazulevicius, *RSC Adv.,* 2016, **6**, 2191.

45 J. Zhou, P. Chen, X. Wang, Y. Wang, Y. Wang, F. Li, M. Yang, Y. Huang, J. Yu and Z. Lu, *Chem. Commun.,* 2014, **50**, 7586.